Revista de la Academia Colombiana de Ciencias Exactas, Físicas y Naturales. 2026
doi: https://doi.org/10.18257/raccefyn.3599

**Physical Sciences**

Original article

# Effect of high-energy ball milling on the structural, morphological, and magnetic properties of FeSiBPCu nanocrystalline soft magnetic alloy

## Efecto de la molienda mecánica de alta energía sobre las propiedades estructurales, morfológicas y magnéticas de la aleación magnética blanda nanocristalina FeSiBPCu

**Darling Perea-Cabarcas[1,2], Indry Milena Saavedra-Gaona[2], Andrés Rosales-Rivera[3], Carlos Arturo Parra-Vargas[2,*], Felix Echeverría[1], Francisco Bolívar[1]**

[1] Centro de Investigación, Innovación de Desarrollo de Materiales – CIDEMAT, Universidad de Antioquia, Medellín, Colombia
[2] Grupo de Física de Materiales (GFM), Universidad Pedagógica y Tecnológica de Colombia, Tunja, Colombia
[3] Laboratorio de Magnetismo y Materiales Avanzados, Facultad de Ciencias Exactas y Naturales, Universidad Nacional de Colombia, Sede Manizales, Manizales, Colombia

## Abstract

We used high-energy ball milling (HEBM) to produce nanocrystalline powders from a FeSiBPCu soft magnetic alloy. We examined the influence of milling time on the structural evolution, particle morphology, and magnetic properties. Our results show that, under the applied milling conditions, the powders reached a steady state characterized by a narrow particle size distribution. The quantitative X-ray diffraction analysis using the Rietveld method revealed a progressive refinement of the α-Fe(Si) crystallite size from 27.6 to 12.8 nm with increasing milling time. Simultaneously, the high mechanical energy input promoted partial crystallization of the residual amorphous phase, leading to the formation of $Fe_5B_2P$ and $Fe_3(B,P)$ secondary phases. The magnetic measurements performed by vibrating sample magnetometry indicated that these microstructural changes significantly affected the magnetic response, resulting in a reduction of saturation magnetization and an increase in coercivity due to milling-induced defects and severe plastic deformation. Despite the degradation of magnetic softness compared to annealed ribbons, the powders obtained retained a typical soft magnetic behavior and properties comparable to Fe-based nanocrystalline powders used in soft magnetic composite cores. These results demonstrate the potential of mechanically processed FeSiBPCu powders for the fabrication of soft magnetic components with complex geometries.

**Keywords:** High energy ball milling; Nanocrystalline alloy; Soft magnetic powders; Structural analysis.

## Resumen

Se empleó molienda mecánica de alta energía (HEBM) para producir polvos nanocristalinos a partir de la aleación magnética blanda FeSiBPCu. La influencia del tiempo de molienda sobre la evolución estructural, la morfología de las partículas y las propiedades magnéticas se investigó de manera sistemática. Los resultados muestran que, bajo las condiciones de molienda aplicadas, los polvos alcanzaron un estado estacionario caracterizado por una distribución estrecha del tamaño de la partícula. El análisis cuantitativo de difracción de rayos X mediante el método de Rietveld reveló un refinamiento progresivo del tamaño del cristalito de la fase α-Fe(Si) de 27,6 a 12,8 nm a medida que aumentó el tiempo de molienda. Simultáneamente, la elevada energía mecánica introducida promovió la cristalización parcial de la fase amorfa residual, dando lugar a la formación de las fases secundarias $Fe_5B_2P$ y $Fe_3(B,P)$. Las mediciones magnéticas mediante magnetometría de muestra vibrante indicaron que estos cambios microestructurales afectaron significativamente la respuesta magnética, resultando en una disminución de la magnetización de saturación y un aumento de la coercitividad debido a los defectos inducidos por la molienda y a una acusada deformación plástica.

**Citation:** Perea-Cabarcas D, *et al.* Effect of high-energy ball milling on the structural, morphological, and magnetic properties of FeSiBPCu nanocrystalline soft magnetic alloy. Revista de la Academia Colombiana de Ciencias Exactas, Físicas y Naturales. 2026 May 6. doi: https://doi.org/10.18257/raccefyn.3599

**Editor:** Rafael González Hernández

***Corresponding autor:**
Carlos Arturo Parra-Vargas;
carlos.parra@uptc.edu.co

**Received:** November 25, 2025
**Accepted:** January 14, 2026
**Published on line:** May 6, 2026

Revista de la Academia Colombiana de Ciencias Exactas, Físicas y Naturales. 2026
doi: https://doi.org/10.18257/raccefyn.3599

A pesar del deterioro de la suavidad magnética en comparación con las cintas recocidas, los polvos obtenidos conservaron el comportamiento magnético blando típico y presentaron propiedades comparables a las de polvos nanocristalinos a base de Fe utilizados en núcleos compuestos magnéticos blandos. Estos resultados demuestran el potencial de los polvos FeSiBPCu procesados mecánicamente para la fabricación de componentes magnéticos blandos con geometrías complejas.

**Palabras clave:** Molienda de alta energía; Aleación nanocristalina; Polvos magnéticos blandos; Análisis estructural.

## Introduction

Iron-based nanocrystalline soft magnetic alloys have attracted sustained scientific and technological interest due to their favorable combination of high permeability, low coercivity, and reduced core losses. Commercial materials such as Finemet, Vitroperm, and Nanoperm, which belong to the Fe–Si–B–Nb–Cu family, are widely used in electromagnetic devices and power electronics applications (**Herzer**, 1996; **Yoshihito Yoshizawa *et al.***, 1994). However, the presence of Nb significantly increases the material cost, limiting the economic competitiveness of these alloys for large-scale applications. In response to this limitation, FeSiBPCu alloys have emerged as a promising alternative, offering good glass-forming ability and the potential to develop nanocrystalline structures with suitable soft magnetic properties after thermal treatment (**Li *et al.***, 2010; **Makino *et al.***, 2009a; **Makino *et al.***, 2009b). Additionally, the use of alloying elements common in the steel industry substantially reduces raw material costs compared to Nb-containing systems. Consequently, FeSiBPCu alloys have been increasingly studied as cost-effective nanocrystalline soft magnetic materials.

Among these, FeSiBPCu nanocrystalline alloys have attracted significant attention due to their relatively high ability to form glass and develop nanocrystalline structures with desirable soft magnetic properties after appropriate thermal processing. The pioneering work by **Makino *et al.*** (2009a) demonstrated that melt-spun FeSiBPCu alloys with heterogeneous amorphous structures containing a high density of α-Fe clusters exhibit high saturation magnetic flux densities ($B_s$ ~1.88–1.94 T) and low coercivity, rivaling commercial crystalline soft magnetic alloys while reducing reliance on expensive alloying elements. More recent studies have further explored compositional optimization within this family, for example, through carbon co-alloying and segmented annealing, which can enhance the amorphous forming ability (AFA), broaden the crystallization window, and improve magnetic performance, achieving $B_s$ values up to ~1.85 T, and significantly improved permeability and reduced core losses (**Chen *et al.***, 2025). Other studies have examined the effects of P and C co-alloying on the glass-forming ability, nanocrystal density, and thermal stability of Fe-based nanocrystalline alloys, highlighting the synergistic role of metalloid additions in refining microstructure and enhancing soft magnetic properties (**Xie *et al.***, 2024).

Despite these advances in ribbon-based nanocrystalline alloys, components produced by melt spinning are inherently limited to thin ribbons (typically 20–30 μm thick) and simple geometries, which restrict their utility in applications requiring complex shapes or larger material volumes. Powder-based processing offers a promising alternative by enabling the fabrication of soft magnetic components with complex geometries and tailored properties through powder metallurgy techniques. Such powder-derived soft magnetic composite cores exhibit improved high-frequency performance and flexible design capabilities, as shown in recent studies on nanocrystalline powder cores and soft magnetic composites prepared from mechanically milled powders (**Wang *et al.***, 2024).

Here, we focused on the mechanical production of nanocrystalline Fe–Si–B–P–Cu powders via high-energy ball milling, starting from a $Fe_{77}Si_8B_{10}P_5$ master alloy with a controlled Cu addition following the $(FeSiBPCu)_{100-x}Cu_x$ formulation ($x$ = 0.75 at.%), which preserves the ratio of glass-forming elements and enables the development of a favorable nanocrystalline structure. The evolution of the structural and magnetic properties

induced by ball milling was systematically examined, as it represents an important advance toward the development of Fe-based powder soft magnetic cores with enhanced design flexibility and magnetic performance.

## Materials and methods

The amorphous alloy $(Fe_{77}\ Si\ _{8}B_{10}P_{5})_{99.25}Cu_{0.75}$ (at. %) was obtained by melt spinning and heat-treated using isothermal annealing at 798K to develop a structure consisting of nanocrystals of α-Fe(Si) embedded in an amorphous matrix. The annealed sample was ground in a Retsch Emax high-energy ball mill using zirconia balls in zirconia-coated stainless-steel containers, maintaining a 5:1 ball/powder weight ratio. The grinding was done in two stages: first, we ground at 1000 r.p.m. for 5 hours using 10 mm balls, and then at 1000 r.p.m. using 3 mm balls for 3 hours. The Emax mill has a cooling system for the grinding vessels and a temperature sensor that warns about overheating during the process, which we set at a limit of 323 K to regulate the temperature of the containers. The grinding was conducted in 15-minute cycles with 5-minute breaks between them to facilitate heat extraction, reversing the direction of rotation in each cycle to avoid agglomeration. Within these operating parameters, the highest temperature recorded was 311.15 K.

To avoid the material from reacting with oxygen, which would cause its oxidation, and to prevent a pyrophoric behavior due to its high phosphorus content, both grinding processes were conducted in a high-purity argon atmosphere by handling the grinding jars and powders in a glove box. To prevent contamination of the material and, thus, introduce defects that could alter its properties, no process-control agent was used.

The annealing temperature was determined from a thermal analysis that identified the characteristic temperatures of the amorphous alloy in a TA Instruments SDT Q600 differential scanning calorimeter (DSC) equipped with a DSC-TGA module. The analysis was performed in the presence of a continuous argon flow of 100 ml/min through the heating chamber at a rate of 20 K/min.

The formation of the amorphous phase, the structural evolution, and the development of the crystalline phases during the heat treatment and subsequent grinding of the ribbons were evaluated by transmission electron microscopy (TEM) and X-ray diffraction (XRD). Here, we used the standard reflection mode in a PANalytical Empyrean diffractometer configured with Bragg-Brentano geometry and equipped with a Co-Kα source ($\lambda$ = 0.178897 Å). The same conditions were applied for all samples: voltage: 40kV, current: 40mA, and interval to record the diffraction intensities (2θ) between 30 and 110 degrees, with a 0.02° step. XRD patterns were analyzed using the General Structure Analysis System (GSAS) software.

The morphology and size distribution estimation of the milled nanocrystalline alloy was studied using a JEOL JSM-6490LV scanning electron microscope (SEM. The particle size distribution was measured from SEM analysis using the ImageJ software. The hysteresis loops were recorded at 300 K between -20 kOe and 20 kOe in a Quantum Design vibrating sample magnetometer (VSM).

## Results and discussion

The DSC analysis curve of the amorphous alloy obtained by melt spinning (**Figure 1a**) shows the two crystallization peaks characteristic of amorphous Fe-based alloys, which have the ability to develop nanocrystalline structures (**Willard & Daniil**, 2013). The annealing process was conducted at 798 K as indicated by the dotted line between the two crystallization peaks; at this temperature, only the precipitation of the phase that crystallizes in the first thermal event is expected to occur, in this case, the α-Fe (Si) phase.

**Figure 1b** shows the XRD patterns of the as-cast and annealed samples. The as-cast sample shows no characteristic diffraction peaks; instead, it exhibits a broad halo, indicating an amorphous structure. The successful formation of the amorphous state by rapid cooling can be attributed to the alloy design, which satisfied the three empirical

Revista de la Academia Colombiana de Ciencias Exactas, Físicas y Naturales. 2026
doi: https://doi.org/10.18257/raccefyn.3599

rules proposed by **Inoue** (2000). In contrast, the heat-treated sample exhibited diffraction peaks corresponding to the α-Fe(Si) phase (ICSD 98-063-3555), with a lattice parameter of 2.8560 Å, slightly lower than that of pure Fe (2.8660 Å). This reduction reflected the diffusion of smaller Si atoms into the α-Fe(Si) lattice, leading to a decrease in the lattice parameter a. Furthermore, the addition of Cu to the base FeSiBP alloy promoted the nucleation and growth of the α-Fe(Si) solid solution during the first crystallization stage, while suppressing the formation of intermetallic compounds such as $Fe_2B$ and $Fe_3(B,P)$ (**Herzer**, 1997; **Li *et al.***, 2010; **Yoshizawa & Yamauchi**, 1990).

**Figure 2a** displays the XRD patterns of the $(Fe_{77}Si_8B_{10}P_5)_{99.25}Cu_{0.75}$ (at. %) powders at different grinding times and ball diameters, showing the occurrence of two simultaneous phenomena, one of which includes the appearance of two crystalline phases different from the α-Fe(Si) obtained by heat treatment, identified as $Fe_3(B,P)$ (ICSD 98-061-4141) and

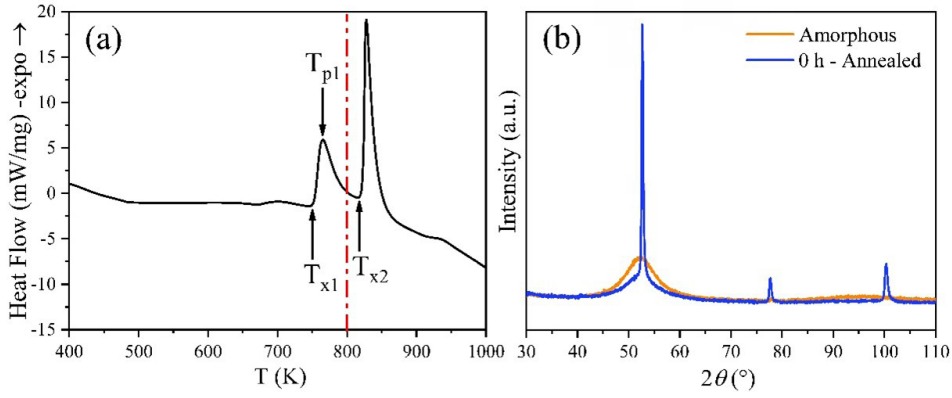


**Figure 1. (a)** DSC analysis of ribbons. **(b)** XRD patterns of amorphous (as-cast) and annealed sample at 798K

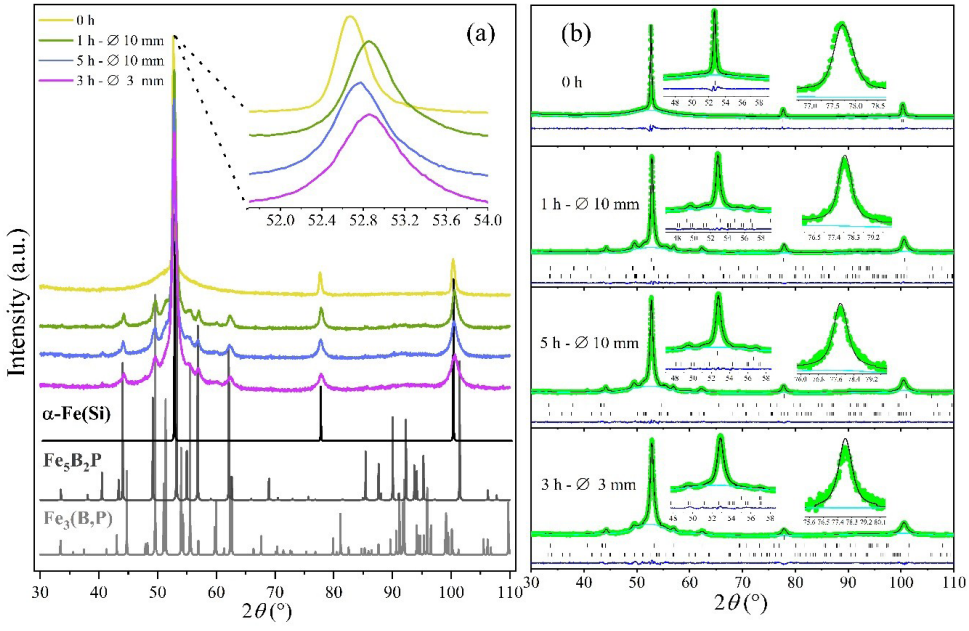


**Figure 2. (a)** XRD patterns of $(Fe_{77}Si_8B_{10}P_5)_{99.25}Cu_{0.75}$ compound. Inset: Enlarged region of the main signal in the $2\theta$ 51.7 – 54.0° range. **(b)** Refinement Rietveld for all powders; experimental pattern (• green), calculated pattern (black line), background (cyan line), difference (blue line) and Bragg position ( | )

$Fe_5B_2P_1$ (ICSD 98-060-1531). These two phases are formed from the remaining amorphous phase as a consequence of the energy transmitted to the material by the impact of the balls (**Koch**, 1997). The energy transmitted to the material can produce local temperature increases associated with shear bands due to the effect of the plastic deformation process (**Huang *et al.***, 1995), or to an improvement in diffusion due to the deformation induced in the material that produces the decomposition of the metastable phase, the latter being considered the most feasible method (**Kwon *et al.,*** 2010; **Ramasamy *et al.***, 2017; **Trudeau**, 1994; **Zhang *et al***., 2008). The other phenomenon observed was the deformation of the crystalline phase present in the material, i.e., the widening and intensity reduction of the α-Fe (Si) phase peaks. This behavior is also observed in amorphization processes and mechanical alloying by milling, where the widening and intensity reduction of the peaks arise as an effect of the decrease in crystallite size and the accumulation of micro-strains due to the continuous deformation to which the material is subjected (**Bahrami *et al.***, 2006; **Eckert *et al.***, 1993; **Nowroozi & Shokrollahi**, 2013; **Surinach *et al.***, 1991; **Suryanarayana**, 2001). To avoid the crystallization of unwanted phases, an option would be the use of powders obtained from the grinding of amorphous ribbons. However, authors such as **Zhang *et al.*** (2013) have shown that the use of powders obtained from as-cast ribbons is not recommended because it requires a high-energy milling process that considerably deteriorates the magnetic properties of the material compared to the powders obtained from annealed ribbons.

The inset in **Figure 2a** shows the magnified region of the main signal corresponding to the (110) plane of the α-Fe (Si) phase in the 52° to 54° 2 θ range. The intensity reduction of the signals obtained, the observed shift toward higher 2 θ values, and the broadening of the peaks (increase in FWHM) at longer milling times demonstrate the unit cell size reduction of the α-Fe (Si) phase. Here, we employed the Rietveld refinement method using the GSAS software to confirm and quantify the identified phases; we also evaluated the various structural parameters. The refined patterns in **Figure 2b** show that the fit parameters ($\chi^2$ and $R(F^2)$) confirmed the stability of the phases, which was evident given that the best fit to the experimental data is confirmed by a Chi-square factor ($\chi^2$) value close to 1.4 and an unweighted structure factor ($R(F^2)$) of around 10%. Our results evidenced, therefore, an excellent agreement between calculation and observation, indicating a good refinement of the identified structures.

**Table 1** summarizes the structural parameters obtained from Rietveld refinement and complementary estimation methods. The lattice parameters (*a*, *b*, and *c*), phase fractions, and unit cell volume were determined by this refinement, while the degree of crystallinity was calculated from the ratio between the integrated area of crystalline peaks and the total area of both the crystalline and amorphous contributions, as defined in equation 1.

$$Degree\ of\ Crystalinity\ (\%) = \frac{Area\ of\ crystalline\ region}{Total\ area\ (crystalline + amorphous)} \times 100 \quad (1)$$

The average crystallite size, *L*, was calculated using the Scherrer estimation method:

$$L = \frac{K\lambda}{\beta cos\theta}, \quad (2)$$

where $\lambda$ is the wavelength of the incident beam, $\beta$ is the full width at half maximum (FWHM), $\theta$ is the reflection angle of the most intense signal, and *K* depends on the shape of the crystallite size, which is equivalent to 0.89 assuming a circular grain. The crystallite size was estimated from the measured FWHM values using the Scherrer equation without explicit correction for instrumental broadening; therefore, these values should be considered as approximate and are used mainly for comparative purposes. Using the integral peak breath (average volume) in the Williamson-Hall method, the deformation induced in the powders due to crystal imperfection and distortion was calculated with:

$$\varepsilon = \frac{\beta}{4Tan(\theta)} \quad (3).$$

Revista de la Academia Colombiana de Ciencias Exactas, Físicas y Naturales. 2026
doi: https://doi.org/10.18257/raccefyn.3599

**Table 1.** Structural parameters of the $(Fe_{77}Si_8B_{10}P_5)_{99.25}Cu_{0.75}$ nanocrystalline powders

| Samples | Phases | % Phase | Lattice parameters (Å) | | | Cell volume (Å³) | α-Fe(Si) crystallite size (nm) | Refinement parameters | | Degree of crystallinity (%) | ε (%) |
|---|---|---|---|---|---|---|---|---|---|---|---|
| | | | *a* | *b* | *c* | | | $\chi^2$ | R($F^2$) | | |
| **0h** | **α-Fe(Si)** | 100 | 2.860 (8) | | | 23.386 (2) | 27.6 | 1.563 | 0.0350 | 73.70 | 0.33 |
| **1h - Ø10 mm** | **α-Fe(Si)** | 69 | 2.856 (1) | | | 23.259 (3) | 18.2 | 1.035 | 0.0802 | 89.99 | 0.49 |
| | **$Fe_5B_2P$** | 17 | 5.557 (7) | 10.467 (1) | | 323.212 (1) | | | | | |
| | **$Fe_3$(B,P)** | 14 | 8.727 (4) | 4.295 (2) | | 327.143 (4) | | | | | |
| **5h - Ø 10 mm** | **α-Fe(Si)** | 69 | 2.852 (7) | | | 23.206 (2) | 15.6 | 1.094 | 0.1097 | 93.22 | 0.57 |
| | **$Fe_5B_2P$** | 12 | 5.514 (6) | 10.375 (1) | | 315.438 (1) | | | | | |
| | **$Fe_3$(B,P)** | 19 | 8.777 (2) | 4.352 (1) | | 335.220 (3) | | | | | |
| **3h - Ø 3 mm** | **α-Fe(Si)** | 76 | 2.852 (4) | | | 23.207 (1) | 12.8 | 1.258 | 0.1391 | 94.56 | 0.69 |
| | **$Fe_5B_2P$** | 15 | 5.478 (7) | 10.320 (2) | | 309.687 (0) | | | | | |
| | **$Fe_3$(B,P)** | 9 | 8.859 (1) | 4.269 (9) | | 335.039 (1) | | | | | |

According to the structural parameters obtained by the refinement shown in **Table 1**, a decrease in lattice parameters *a*, *b*, and *c* was observed in all phases, which is consistent with the displacement at higher angles, resulting in a decrease in cell volume. The reduction in the unit cell volume can be attributed to the severe plastic deformation experienced by the powders, which is characterized by the accumulation of defects and work hardening of the particles as the milling process progresses, embrittling the material and favoring particle fracture. For this reason, a structural analysis would reflect this phenomenon by a reduction in peak intensities corresponding to the crystalline phases and a broadening of the peaks. By increasing the milling time, a structure composed of nanometric grains immersed in an amorphous matrix could be achieved, or the material could even be completely amorphized (**Neamţu *et al.***, 2016).

**Table 1** also shows an increase in the overall percentage of the α-Fe(Si) phase and a decrease in the percentage of the $Fe_3$(B,P) and $Fe_5B_2P_1$ phases in the second stage of the milling process. The broadening of the peaks and the reduction in their intensity suggest a severe plastic deformation in all phases, causing, again, the amorphization of the small grains of the secondary phases. On the other hand, both Scherrer and Rietveld methods revealed the effect of plastic deformation with a reduction in crystallite size of the α-Fe(Si) phase from 27.6 to 12.8 nm in the annealed sample and the second milling stage, respectively.

It is worth noting that during the final milling stage (3 h with 3 mm balls), the continuous shift of the α-Fe(Si) diffraction peaks toward higher 2θ values tended to stabilize, as reflected by the nearly constant lattice parameter observed between the 5 h and 3 h milling conditions. This behavior suggests a competition between two concurrent mechanisms: On the one hand, severe plastic deformation promotes lattice compression through the accumulation of defects and microstrains. On the other hand, the mechanically induced crystallization of the residual amorphous matrix contributes to the formation of new α-Fe(Si) nanocrystals with a less distorted lattice. As a result, the effective lattice parameter reaches a quasi-stationary state, accompanied by an increase of approximately 7% in the volume fraction of the α-Fe(Si) phase, as evidenced by the Rietveld refinement results.

The transmission electron microscopy (TEM) analysis of the annealed alloy showed uniform crystallization. **Figure 3a** shows a high-resolution electron microscopy (HREM) image of one edge of the sample, where a large number of grains ranging from 12 to 40 nm embedded in an amorphous matrix can be observed. This structure formed due to the presence of Cu and P, which determined the crystallization behavior of the alloy during

the decomposition of the amorphous phase, as Cu atoms act as a heterogeneous nucleation site for the α-Fe(Si) phase grains and P stabilizes the amorphous phase by restricting the formation of Fe, B, and P crystalline phases, while limiting the growth of α-Fe(Si) grains (**Cui *et al.,*** 2009; **Makino *et al.***, 2009; **Wang *et al.***, 2011). **Figure 3b** shows the selected area electron diffraction (SAED) pattern, where two slightly diffuse continuous rings can be seen with multiple spots indicating the presence of nanometer crystalline phases. We calculated interplanar distances of 2.008Å and 1.4048Å, corresponding to the (110) and (200) planes of the α-Fe(Si) phase, respectively, by measuring the diameter of the rings and using the equation of the camera constant: $\lambda L = d_{hkl} R$.

Next to the electron microscope beam stopper, a small dot can be observed (indicated with a red arrow), which corresponds to a crystalline plane with an interplanar distance of 2.98 Å, very close to that of plane (112) of the $Fe_3(B,P)$ compound, this being one of the equilibrium phases. We found no other evidence to confirm the presence of this phase, which was neither confirmed by XRD. Its detection was possible because TEM is quite punctual and allows finding detailed phases or compound particles that, due to their size or concentration, cannot be detected by X-ray diffraction. No major evidence of the $Fe_3(B,P)$ compound was found; however, this small plane may mean that during the time the sample was subjected to the thermal treatment, a small amount of this equilibrium phase precipitated from the remaining amorphous phase. In fact, this alloy has a uniform, nanometer-sized grain, but not as small as the grains between 10 and 20 nm reported for Finemet alloys (**Kulik *et al.***, 2005; **Yoshizawa *et al.***, 1988).

The grinding process was followed by SEM analysis. The heat treatment of the amorphous ribbons significantly reduced the mechanical properties of the material, which became brittle, so we were able to crush them manually and introduce them into the grinding jars. The debris obtained had straight edges, revealing a brittle fracture with no plastic deformation, as shown in the SEM image in **Figure 3c**. The first grinding stage

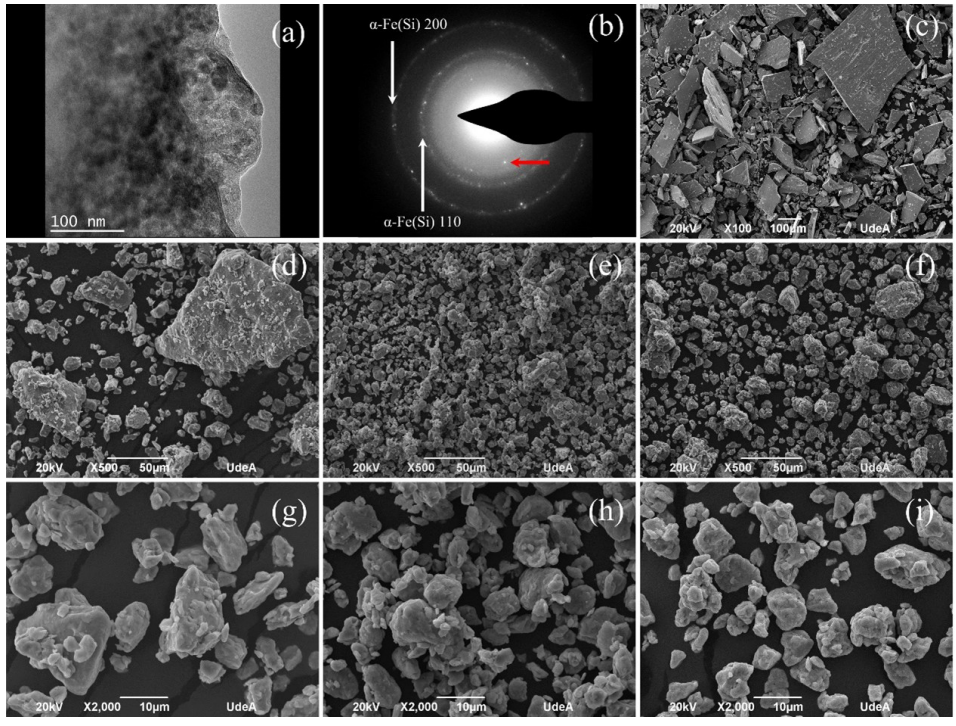


**Figure 3. (a)** TEM image of nanocrystalline alloy after annealing at 798K. **(b)** SAED pattern of annealed sample. **(c-i)** SEM images of powders: **(c)** crushed ribbons, 0h milling; (**d and g**) milled for 1h, 10mm balls; (**e and h**) 5h of milling, 10mm balls; (**f and i**) 3h of milling with 3mm balls

Revista de la Academia Colombiana de Ciencias Exactas, Físicas y Naturales. 2026
doi: https://doi.org/10.18257/raccefyn.3599

consisted of 5 hours using 10 mm diameter balls. After the first hour, the ribbons were destroyed, and 3 to 125 µm-wide particles were obtained, as can be observed in **Figure 3d, g**. After 5 hours of grinding, the particle size was reduced to a narrower range of 1 to 20 µm with a mean value of 6 µm (**Figure 3e, h**). As a result of the plastic deformation to which the material was subjected, the particles obtained had a ductile appearance with rounded edges, and the particle agglomerates began to form. In the second stage of the milling process, we used 3-mm grinding bodies to disaggregate the agglomerates formed and continued the size reduction. The results after 3 hours of grinding with 3 mm balls are shown in **Figure 3f, i**, where the predominant mechanism is the size reduction, reaching a range of 0.9 to 24 µm. However, longer times resulted in particle agglomeration, leading to a variation in the size distribution towards values greater than those observed at the end of the first stage. At this point, the predominant phenomenon was the growth of particle size from the cold welding of the smallest particles. Such growth occurred because, during the fracture of the fragilized particles due to the high degree of plastic deformation, fracture surfaces were created that favor cold welding with other newly created surfaces. After, the steady state was reached and the rate at which the particles were welded together equaled the rate at which they were fractured, narrowing the size distribution range (**Benjamin**, 1976; **Benjamin & Volin**, 1974; **Suryanarayana *et al.***, 2001).

**Figure 4** shows the isotherms of the $(Fe_{77}Si_8B_{10}P_5)_{99.25}Cu_{0.75}$ (at.%) powders at room temperature and different milling times. The powders exhibited typical soft magnetic properties, high saturation magnetization (Ms), and low coercivity (Hc). The insets show the variation of Ms, Hc, and a magnification of the hysteresis loops. The coercivity of the samples underwent a sharp increase at the beginning of the process and maintained an almost constant value until the end, while Ms decreased as the milling time increased. On the other hand, magnetization increased sharply with the applied magnetic field (H) for H<5.0 kOe and then gradually reached saturation, indicating ferromagnetic behavior. As shown in the figure, the sample with 0h (annealed, no grinding) had the highest flux density at the same applied magnetic field strength (H). The saturation magnetization for the samples with 1 and 5 h of grinding with 10 mm balls was similar, Ms being slightly higher with 5-hour grinding than with 1 h. On the other hand, Ms for the sample with 3 h-grinding and 3 mm balls was lower compared to the other samples' Ms.

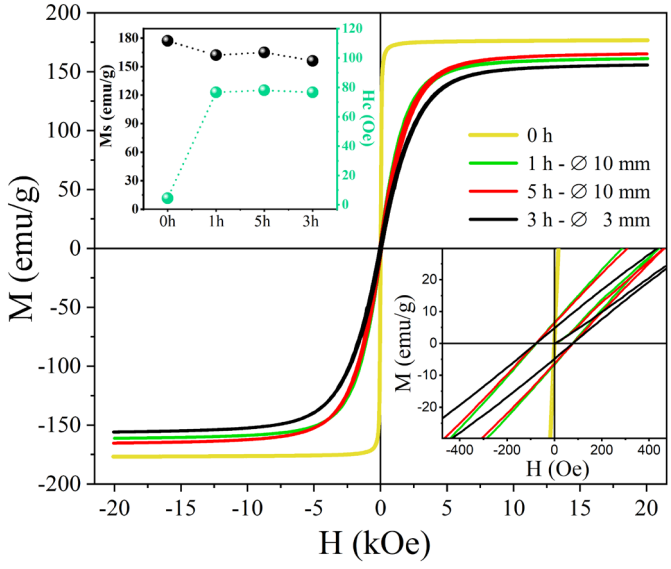


**Figure 4.** Hysteresis loops of $(Fe_{77}Si_8B_{10}P_5)_{99.25}Cu_{0.75}$ nanocrystalline powders at 300 K. Magnetic parameters Ms and Hc as a function of milling time (upper left inset) and extended hysteresis loops (lower right inset)

The coercive field of powders is mainly influenced by the plastic deformations they undergo during milling. The smaller particles have a higher content of structural defects related to their size than larger ones, which leads to an improvement in domain-wall attachment and is the main reason for the increase in coercive field (**Huang *et al.***, 2015; **Nowosielski *et al.***, 2005; **Nuetzel *et al.***, 1999). Another effect of milling on the magnetic properties is the reduction in permeability with particle size; however, in the fabrication of devices from powders, a small particle size with an adequate amount of binder can improve core performance at high frequency (**Nuetzel *et al.***, 1999).

The hysteresis loop onset slope for 1 h and 5 h was relatively the same, and was less than that of the annealed sample (with 0 h) but greater than that for 3 h of grinding with 3 mm balls. This indicates that the annealed sample was softer than the others, whose domains are more easily oriented with the applied magnetic field, i.e., the domain walls move more easily with the field. Phase formation with boron and phosphorus, Fe3(B, P) and Fe5B2P, reduced the soft magnetic properties, maybe associated with an increase in the magneto-elastic anisotropy in the powders obtained, which was more significant in the 3h-milling sample with 3mm balls. In other words, in the annealed sample, with no phase formation with B and P, the α-Fe(Si) phase was predominant at the nanoscale level, favoring the good soft magnetic behavior, i.e., the formation of these secondary phases degraded the good soft magnetic behavior (**Le *et al.,*** 2006).

We must emphasize that the degradation observed in the DC magnetic properties, namely the increase in coercivity and the reduction in saturation magnetization, represents an intrinsic physical trade-off associated with the powder processing route. The severe plastic deformation and particle isolation required to obtain free-flowing powders inevitably introduce defects and interparticle boundaries that affect magnetic softness. However, this powder morphology enables the consolidation of the material into soft magnetic cores with complex geometries and electrically insulated particles. Such characteristics are crucial for high-frequency (AC) applications, as they significantly reduce eddy current losses, which are the dominant loss mechanism in bulk or ribbon-based materials. Therefore, the mechanically processed FeSiBPCu powders are better suited for high-frequency applications, primary industrial use of soft magnetic powder cores, despite the deterioration in DC magnetic properties.

The magnetic behavior of the $(Fe_{77}Si_8B_{10}P_5)_{99.25}Cu_{0.75}$ (at.%) powders processed by high-energy ball milling showed both similarities and clear differences compared with FeSiBPCu nanocrystalline alloys reported in recent literature. For melt-spun FeSiBPCu ribbons subjected to optimized heat treatments, saturation magnetization values in the range of 1.85-1.94 T and coercivities below 10 A/m have been reported, which are attributed to the formation of a homogeneous nanocrystalline α-Fe(Si) structure with low defect density and minimal magnetoelastic anisotropy (**Makino *et al.***, 2009). In contrast, the powders we obtained exhibited lower $M_s$ and higher $H_c$, which is consistent with the fundamentally different processing route based on mechanical milling.

Recent studies on FeSiBPCu alloys modified by carbon addition or segmented annealing have shown that careful control of crystallization kinetics can preserve high Bs while maintaining low coercivity by suppressing secondary phase formation (**Chen *et al.***, 2025). Unlike these thermally optimized ribbon-based systems, the mechanical energy introduced during ball milling in the present study promoted partial crystallization of the residual amorphous phase into $Fe_3(B,P)$ and $Fe_5B_2P$ phases. Similar phase transformations induced by high-energy milling have been reported in FeBP-based nanocrystalline powders, where the appearance of boron- and phosphorus-rich phases has led to a reduction in saturation magnetization and an increase in coercivity due to enhanced magnetoelastic anisotropy and domain wall pinning.

Although the magnetic performance of the powders we obtained was inferior to that of ribbon-based FeSiBPCu nanocrystalline alloys, it is comparable to values reported for Fe-based nanocrystalline powders used in powder core applications, where a compromise between magnetic softness and processability is unavoidable. Recent studies on soft

Revista de la Academia Colombiana de Ciencias Exactas, Físicas y Naturales. 2026
doi: https://doi.org/10.18257/raccefyn.3599

magnetic powder cores emphasize that reduced permeability and increased coercivity at the powder level can be partially compensated at the component level by appropriate particle size control, insulation, and binder content, leading to improved high-frequency performance (**Nützel *et al.***, 1999; **Hu *et al.***, 2024). In this sense, the present work extends the FeSiBPCu alloy concept from ribbons to powders, providing experimental evidence that mechanically processed FeSiBPCu powders retain ferromagnetic behavior and constitute a viable starting material for advanced soft magnetic core fabrication.

## Conclusions

The experimental results showed that a combined process involving the controlled thermal decomposition of the amorphous phase in the $(Fe_{77}Si_8B_{10}P_5)_{99.25}Cu_{0.75}$ (at.%) amorphous alloy, followed by a high-energy ball milling, provided a route to obtain metallic powders with a high content of α-Fe(si) nanocrystalline grains embedded in an amorphous matrix. The steady state was the determining factor in the success of powder processing. No significant changes in particle-size distribution were observed between 5h grinding with 10 mm balls and 3h grinding with 3 mm balls; however, the second grinding stage showed a reduction in the soft magnetic properties of the material. Structural defects induced during the high-energy ball milling process in the α-Fe(Si) phase and the formation of $Fe_3(B, P)$ and $Fe_5B_2P$ caused a slight deterioration of magnetic properties compared with the as-annealed ribbons. The structure obtained adequately combines high saturation magnetization and low coercive field, making it a promising candidate for the fabrication of soft magnetic powder cores.

Our results confirmed that thermal treatment combined with high-energy ball milling enables the production of FeSiBPCu nanocrystalline powders with a high fraction of α-Fe(Si) embedded in an amorphous matrix. Compared to commercial ribbon-based nanocrystalline alloys, such as Finemet or Vitroperm, the powders obtained exhibited lower saturation magnetization and higher coercivity, mainly attributed to milling-induced structural defects and the formation of $Fe_3(B,P)$ and $Fe_5B_2P$ secondary phases. Despite this reduction in magnetic softness, the magnetic properties achieved are comparable to those reported for Fe-based nanocrystalline powders used in soft magnetic composite cores, where powder processability and geometrical flexibility are prioritized over maximum magnetic performance, which highlights the relevance of the proposed processing route for applications requiring complex-shaped magnetic components. Future works will focus on optimizing milling parameters and post-milling thermal treatments to suppress secondary phase formation and reduce defect density, and on the fabrication and evaluation of consolidated powder cores to assess their performance under high-frequency operating conditions.

## Data availability statement

The data used are presented in the manuscript.

## Acknowledgments

We want to thank the Ministerio de Ciencia, Tecnología e Innovación for the support received through its call for proposals 891 of 2020, mechanism 2, and the Universidad Pedagógica y Tecnológica de Colombia – UPTC, for its administrative support and resource administration.

## Author contributions

D.P.: Experimental work, analysis of results, writing of the manuscript. I.M.S.: XRD analysis and refinement. A.R. VSM measurement and analysis. C.A.P.: Supervision and revision of the manuscript. F.B.: Discussion, analysis of results, and revision of the manuscript. F.E.: Discussion, analysis of results, and revision of the manuscript. All authors have read and agreed to the published version of the manuscript.

## Conflicts of interests

The authors declare no conflict of interest.

## References

**Bahrami, A., Madaah Hosseini, H. R., Abachi, P., Miraghaei, S.** (2006). Structural and soft magnetic properties of nanocrystalline Fe85Si10Ni5 powders prepared by mechanical alloying. *Materials Letters*, *60*(8), 10681070. https://doi.org/10.1016/j.matlet.2005.10.078

**Benjamin, J. S.** (1976). Mechanical alloying. *Scientific American*, *234*, 4049. https://doi.org/10.1038/scientificamerican0576-40

**Benjamin, J. S. & Volin, T. E.** (1974). The mechanism of mechanical alloying. *Metallurgical Transactions*, *5*(8), 19291934. https://doi.org/10.1007/BF02644161

**Chen, X., Zheng, Z., Yu, B., Xiao, B., Qiu, Z., Zeng, D.** (2025). The enhanced soft magnetic properties of FeSiBPCu nanocrystalline alloys by doping C and segmented annealing. *Journal of Alloys and Compounds, 1032*, 181225. https://doi.org/10.1016/j.jallcom.2025.181225

**Cui, L., Men, H., Makino, A., Kubota, T., Yubuta, K., Qi, M., Inoue, A.** (2009). Effect of Cu and P on the Crystallization Behavior of Fe-Rich Hetero-Amorphous FeSiB Alloy. *Materials Transactions*, *50*(11), 25152520. https://doi.org/10.2320/matertrans.M2009206

**Eckert, J., Holzer, J. C., Krill, C. E., Johnson, W. L.** (1993). Mechanically driven alloying and grain size changes in nanocrystalline Fe-Cu powders. *Journal of Applied Physics*, *73*(6), 27942802. https://doi.org/10.1063/1.353055

**Herzer, G.** (1996). Nanocrystalline soft magnetic materials. *Journal of Magnetism and Magnetic Materials*, *157158*, 133136. https://doi.org/10.1016/0304-8853(95)01126-9

**Herzer, G.** (1997). Nanocrystalline soft magnetic alloys. Dans K. H. J. Buschow (Ed), *Handbook of Magnetic Materials* (vol. 10, p. 415462). Elsevier Science B.V. https://doi.org/10.1016/S1567-2719(97)10007-5

**Huang, B., Pérez, R. J., Crawford, P. J., Sharif, A. A., Nutt, S. R., Lavernia, E. J.** (1995). Mechanically induced crystallization of metglas Fe78B13Si9 during cryogenic high energy ball milling. *Nanostructured Materials*, *5*(5), 545553. https://doi.org/10.1016/0965-9773(95)00261-C

**Huang, Cb., Liu, Tc., Wang, Xy., Lu, Cw., Li, Dr., Lu, Zc.** (2015). Magnetic properties of nanocrystalline powder cores fabricated by mechanically crushed powders. *Journal of Iron and Steel Research International*, *22*(1), 6771. https://doi.org/10.1016/S1006-706X(15)60011-5

**Idzikowski, B., Švec, P., Miglierini, M. (Ed.).** (2005). Nanocrystalline Alloys from Amorphous Precursors. Proceedings of the NATO Advanced Research Workshop on Properties and Applications of Nanocrystalline Alloys from Amorphous Precursors, Budmerice. *Springer Dordrecht.* https://doi.org/10.1007/1-4020-2965-9

**Inoue, A.** (2000). Stabilization of metallic supercooled liquid and bulk amorphous alloys. *Acta Materialia*, *48*(1), 279306. https://doi.org/10.1016/S1359-6454(99)00300-6

**Koch, C. C.** (1997). Synthesis of nanostructured materials by mechanical milling: problems and opportunities. *Nanostructured Materials*, *9*(18), 1322. https://doi.org/10.1016/S0965-9773(97)00014-7

**Kulik, T., Ferenc, J., Kowalczyk, M., Xiubing, L., Nedelko N.** (2005). Magnetically Soft Nanocrystalline Materials Obtained by Devitrification of Metallic Glasses. *Journal of Magnetics, 9, 65–8.* https://doi.org/10.4283/JMAG.2004.9.2.065Kulik

**Kwon, Y.-S., Kim, J.-S., Kim, J.-C., Kwon, Y.-J., Povstugar, I., Yelsukov, E., Kim, C.-E., Lee, H.-S.** (2010). Crystallization of Amorphous Fe 90Zr 10 under ball milling. *Journal of Nanoscience and Nanotechnology*, *10*(1), 336339. https://doi.org/10.1166/jnn.2010.1527

**Le, A. T., Kim, C. O., Chau, N., Duy Cuong, N., Duc Tho, N., Quang Hoa, N., Lee, H.** (2006). Soft magnetic properties and giant magneto-impedance effect of Fe73.5-xCrxSi13.5B9Nb3Au1 (x=1-5) alloys. *Journal of Magnetism and Magnetic Materials*, *307*(2), 178185. https://doi.org/10.1016/j.jmmm.2006.03.066

**Li, X., Kato, H., Yubuta, K., Makino, A., Inoue, A.** (2010). Effect of Cu on nanocrystallization and plastic properties of FeSiBPCu bulk metallic glasses. *Materials Science and Engineering A*, *527*(1011), 25982602. https://doi.org/10.1016/j.msea.2009.12.026

**Makino, A., Li, X., Yubuta, K., Chang, C., Kubota, T., Inoue, A.** (2009a). The effect of Cu on the

plasticity of Fe-Si-B-P-based bulk metallic glass. *Scripta Materialia*, *60*(5), 277280. https://doi.org/10.1016/j.scriptamat.2008.09.008

**Makino, A., Men, H., Kubota, T., Yubuta, K., Inoue, A.** (2009b). FeSiBPCu Nanocrystalline Soft Magnetic Alloys with High Bs of 1.9 Tesla Produced by Crystallizing Hetero-Amorphous Phase. *Materials Transactions*, *50*(1), 204209. https://doi.org/10.2320/matertrans.MER2008306

**Makino, A., Men, H., Yubuta, K., Kubota, T.** (2009c). Soft magnetic FeSiBPCu heteroamorphous alloys with high Fe content. *Journal of Applied Physics*, *105*(1), 15. https://doi.org/10.1063/1.3060579

**Makino, A., Men, H., Kubota, T., Yubuta, K., Inoue, A.** (2009d). New Fe–metalloids–based nanocrystalline alloys with high *Bs* of 1.9 T and excellent magnetic softness. *Journal of Applied Physics, 105*(7), 07A308. https://doi.org/10.1063/1.3058624

**Neamțu, B. v., Chicinaș, H. F., Marinca, T. F., Isnard, O., Pană, O., Chicinaș, I.** (2016). Amorphisation of Fe-based alloy via wet mechanical alloying assisted by PCA decomposition. *Materials Chemistry and Physics*, *183*, 8392. https://doi.org/10.1016/j.matchemphys.2016.08.005

**Nowosielski, R., Wysłocki, J. J., Wnuk, I., Sakiewicz, P., Gramatyka, P.** (2005). Ferromagnetic properties of polymer nanocomposites containing Fe 78Si9B13 powder particles. *Journal of Materials Processing Technology*, *162163* (SPEC. ISS.), 242247. https://doi.org/10.1016/j.jmatprotec.2005.02.010

**Nowroozi, M. A. & Shokrollahi, H.** (2013). Magnetic and structural properties of amorphous/nanocrystalline Fe 42Ni28Zr8Ta2B10C 10 soft magnetic alloy produced by mechanical alloying. *Advanced Powder Technology*, *24*(6), 11001108. https://doi.org/10.1016/j.apt.2013.03.016

**Nuetzel, D., Rieger, G., Wecker, J., Petzold, J., Mueller, M.** (1999). Nanocrystalline soft magnetic composite-cores with ideal orientation of the powder-flakes. *Journal of Magnetism and Magnetic Materials*, *196*, 327329. https://doi.org/10.1016/S0304-8853(98)00736-7

**Ramasamy, P., Shahid, R. N., Scudino, S., Eckert, J., Stoica, M.** (2017). Influencing the crystallization of Fe 80 Nb 10 B 10 metallic glass by ball milling. *Journal of Alloys and Compounds*, *725*, 227236. https://doi.org/10.1016/j.jallcom.2017.07.160

**Surinach, S., Baro, M. D., Segura, J., Clavagueramora, M. T., Clavaguera, N.** (1991). Amorphization of Soft Magnetic-Alloys by the Mechanical Alloying Technique. *Materials Science And Engineering A-Structural Materials Properties Microstructure And Processing*, *134*, 13681371. https://doi.org/10.1016/0921-5093(91)90992-V

**Suryanarayana, C.** (2001). Mechanical alloying and milling. *Progress in Materials Science*, *46*(12), 1184. https://doi.org/10.1016/S0079-6425(99)00010-9

**Suryanarayana, C., Ivanov, E., Boldyrev, V. V.** (2001). The science and technology of mechanical alloying. *Materials Science and Engineering: A*, *304*, 151158. https://doi.org/10.1016/S0921-5093(00)01465-9

**Trudeau, M. L.** (1994). Deformation induced crystallization due to instability in amorphous FeZr alloys. *Applied Physics Letters*, *64*(26), 36613663. https://doi.org/10.1063/1.111953

**Wang, A. D., Men, H., Shen, B. L., Xie, G. Q., Makino, A., Inoue, A.** (2011). Effect of P on crystallization behavior and soft-magnetic properties of Fe83.3Si4Cu0.7B12-xPx nanocrystalline soft-magnetic alloys. *Thin Solid Films*, *519*(23), 82838286. https://doi.org/10.1016/j.tsf.2011.03.110

**Wang, P., Zhu, Z., Liu, J., Wang, H., Pang, J., Zhang, J.** (2024). Finemet nanocrystalline magnetic powder cores: Application of binder and warm compaction process. *Journal of Magnetism and Magnetic Materials, 596*, 171985. https://doi.org/10.1016/j.jmmm.2024.171985

**Willard, M. A. & Daniil, M.** (2013). *Nanocrystalline Soft Magnetic Alloys Two Decades of Progress*. *Handbook of Magnetic Materials* (1re éd., vol. 21). Elsevier B.V. https://doi.org/10.1016/B978-0-444-59593-5.00004-0

**Xie, L., Li, Q., Chang, C., Fan, X., He, A., Cai, Y., Dong, Y.** (2024). Influence of P and C co-alloying on soft magnetic properties and crystallization behavior of FeSiBPCCu nanocrystalline alloys. *Journal of Materials Research and Technology, 33*, 3106-3116. https://doi.org/10.1016/j.jmrt.2024.10.030

**Yoshizawa, Y, Oguma, S., Yamauchi, K.** (1988). New Fe-based soft magnetic alloys composed of ultrafine grain structure. *Journal of Applied Physics*, *64*(10), 60446046. https://doi.org/10.1063/1.342149

**Yoshizawa, Y. & Yamauchi, K.** (1990). Fe-based soft magnetic alloys composed of ultrafine

grain structure. *Materials Transactions, JIM*, *31*(4), 307314. https://doi.org/10.2320/matertrans1989.31.307

**Yoshizawa, Y., Bizen, Y., Arakawa, S.** (1994). Magnetic properties of FeCuNbSiB nanocrystalline alloys with low magnetostriction. *Materials Science and Engineering A*, *181182*(C), 871875. https://doi.org/10.1016/0921-5093(94)90759-5

**Zhang, C., Zhang, Z., Qi, Z., Qi, Y., Zhang, J., Bian, X.** (2008). Ball milling induced abnormal crystallization behavior of an amorphous Fe78Si9B13 alloy, *354*, 38123816. https://doi.org/10.1016/j.jnoncrysol.2008.05.003

**Zhang, Y., Sharma, P., Makino, A.** (2013). Sintered powder cores of high Bsand low coreloss Fe 84.3Si4B8P3Cu0.7 nano-crystalline alloy. *AIP Advances*, *3*(6), 013. https://doi.org/10.1063/1.4811465